Journal of The Electrochemical Society, **152** (9) H146-H151 (2005)
0013-4651/2005/152(9)/H146/6/$7.00 © The Electrochemical Society, Inc.

Sol-gel Synthesis and Characterization of Zn_2SiO_4:Mn@SiO_2 Spherical Core-Shell Particles

D. Y. Kong,[a] M. Yu,[a,b] C. K. Lin,[a] X. M. Liu,[a] J. Lin,[a,z] and J. Fang[c]

[a]*Key Laboratory of Rare Earth Chemistry and Physics, Changchun Institute of Applied Chemistry, Chinese Academy of Sciences, Changchun 130022, and Graduate School of the Chinese Academy of Sciences, Beijing 100049, China*
[b]*Department of Chemistry, Northeast Normal University, Changchun 130024, China*
[c]*Department of Chemistry and Advanced Materials Research Institute, University of New Orleans, New Orleans, Louisiana 70148, USA*

The synthesis and characterization of Zn_2SiO_4:Mn phosphor layers on spherical silica spheres, i.e., core-shell particles of Zn_2SiO_4:Mn@SiO_2 are described in this paper. First, monodisperse silica spheres with an average size around 750 nm have been obtained via the Stöber method by the hydrolysis and condensation of tetraethoxysilane $Si(OC_2H_5)_4$ under base condition (using NH_4OH as the catalyst). Second, the silica spheres are coated with Zn_2SiO_4:Mn phosphor layers by a sol-gel process. The resulting core-shell particles are characterized by X-ray diffraction, Fourier transform infrared spectroscopy, field emission scanning electron microscope, energy-dispersive X-ray spectroscopy, transmission electron microscopy, photoluminescence, low-voltage cathodoluminescence, as well as kinetic decay. The results confirm that the 1000°C-annealed sample consists of crystalline Zn_2SiO_4:Mn shells and amorphous SiO_2 cores with spherical morphology and narrow size distribution. The Zn_2SiO_4:Mn@SiO_2 particles show the green emission at 521 nm corresponding to $^4T_1(^4G)$-$^6A_1(^6S)$ transition of Mn^{2+} under the excitation of UV (250 nm), vacuum UV (172 nm), and electron-beams (1–6 kV). The luminescence intensity has been studied as a function of coating number, accelerating voltage, and filament current, respectively.
 [DOI: 10.1149/1.1990612]

Manuscript submitted January 24, 2005; revised manuscript received April 13, 2005. Available electronically July 28, 2005.

The core-shell composite particles are of extensive scientific and technological interest due to the ability to fine-tune their properties.[1-5] Core-shell materials consist of a core structural domain covered by a shell domain. The core and shell domains may be composed of a variety of materials including polymers, inorganic solids, and metals. The structure, size, and composition of these particles can be easily altered in a controllable way to tailor their magnetic, optical, mechanical, thermal, electrical, electro-optical, and catalytic properties.[1-8] Until now, many routes have been developed to fabricate such core-shell materials, such as the sol-gel process,[1] layer-by-layer technique,[9] template directed self-assembly,[10] and encapsulation of silica nanoparticles by in situ polymerization.[11]

The demand for high resolution and increased efficiency in phosphors for cathode ray tubes (CRTs) and field emissive displays has promoted the development of phosphors that perform at low voltages.[12] In particular, phosphors made up of small, ideally spherical particles are of interest because they offer the possibility of brighter cathodoluminescent performance, high definition, and much improved screen packing.[13] The ideal morphology of phosphor particles includes a perfect spherical shape, narrow size distribution (0.5–3 μm), and nonagglomeration. Spherical morphology of the phosphors is good for high brightness and high resolution. Additionally, high packing densities and low scattering of light can also be obtained by using spherical phosphors. Nowadays, many synthetic routes have been developed to control the size and distribution of phosphor particles, such as spray pyrolysis[14,15] and fluxes precipitation.[16]

Silica can be easily made controllably in spherical morphology from nano- to micrometer size.[17] If the silica spheres are coated with layers of phosphors, a kind of core-shell phosphor materials with spherical morphology is obtained, and the size of the phosphor particles can be controlled by the silica cores. Furthermore, because silica is cheaper than most of the phosphor materials, the core-shell phosphor materials are cheaper than the pure phosphor materials in unit mass. Our group has been preparing various kinds of phosphor coatings on bulk silica glass and silicon wafer substrates via the sol-gel process.[18,19] It would be of great interest and importance to check if the core-shell phosphor materials can be prepared in a similar process.

It is well known that Mn^{2+}-doped zinc orthosilicate (α-Zn_2SiO_4, willemite) has been widely used as a green component in plasma display panels (PDPs), CRTs, and electroluminescent devices due to its highly saturated color, strong luminescence, and long lifespan.[20,21] Recently, much attention has been paid to the synthesis and performance of nanostructural Zn_2SiO_4:Mn phosphors by sol-gel, hydrothermal, spray pyrolysis, and combustion methods, etc..[22-26] Interestingly, ZnO nanowires sheathed with Zn_2SiO_4 were reported by Wang's group.[27] Herein, we select Zn_2SiO_4:Mn as the phosphor shells and silica spheres as the cores, respectively, to obtain the core-shell structured Zn_2SiO_4:Mn@SiO_2 materials via the sol-gel process and characterize the structure, morphology, and photoluminescent and cathodoluminescent properties of the resulting samples.

Experimental

The starting materials for the preparation of Zn_2SiO_4:Mn@SiO_2 core-shell phosphors were tetraethoxysilane (TEOS) $Si(OC_2H_5)_4$ (analytical reagent, AR), ammonium hydroxide NH_4OH (AR), zinc acetate dihydrate $Zn(OOCCH_3)_2{\cdot}2H_2O$ (99.99%), manganese acetate tetrahydrate $Mn(OOCCH_3)_2{\cdot}4H_2O$ (99.99%), citric acid monohydrate (AR), polyethylene glycol (PEG, molecular weight 10,000; AR), nitric acid HNO_3 (AR), ethanol C_2H_5OH (AR), and deionized water.

Preparation of monodisperse SiO_2 spheres.—Monodisperse silica spheres were prepared by the Stöber method.[17] Typically, 25.7 mL TEOS was hydrolyzed in 171 mL ethanol in the presence of 196 mL ammonium hydroxide and 7.0 mL deionized water. The obtained silica spheres were centrifugally separated from the suspension and dried in an oven at 100°C for 24 h.

Surface coating of Zn_2SiO_4:Mn layer on SiO_2 spheres.—The doping concentration of Mn^{2+} is 2 mol %, substituting for Zn^{2+} in Zn_2SiO_4 layer, which has been optimized previously.[20-25] Stoichiometric weights of $Zn(CH_3COO)_2{\cdot}2H_2O$ and $Mn(CH_3COO)_2{\cdot}4H_2O$ were dissolved in 50 mL ethanol-water (8:1 in volume) solution in the presence of 1 mL nitric acid under stirring. Citric acid monohydrate as chelating agent (citric acid/metal

[z] E-mail: jlin@ns.ciac.jl.cn

ion = 2:1) and PEG as cross-linking agent were dissolved in the above solution, then silica spheres were added into the solution and the resulting mixture was further stirred for 3 h. The precipitates were filtered and dried at 100°C for 2 h, then preheated at 500°C for 3 h in a furnace with a heating rate of 60°C/h. The preheated samples were annealed to 1000°C at 100°C/h and held there for 3 h. In this way, the core-shell structured Zn_2SiO_4:Mn@SiO_2 materials have been obtained, and the whole process is shown in Scheme

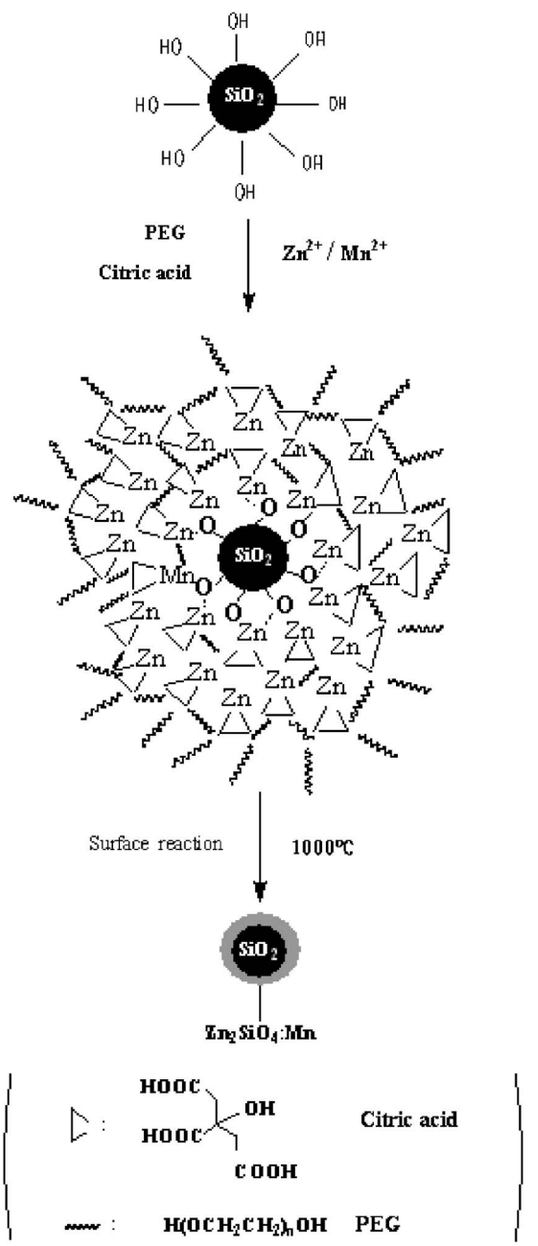

Scheme 1. Formation process of Zn_2SiO_4:Mn@SiO_2 core-shell particles.

1. For multiple coating, the precursor solution is a little different from the above one because the surface of silica spheres were covered by Zn_2SiO_4:Mn layers which could not continue to react with Zn^{2+} and Mn^{2+}. Instead of citric acid and PEG, the stoichiometric weights of TEOS were added as silicon source in the mixing solution of Zn^{2+} and Mn^{2+}; and then the solution was stirred for 2 days

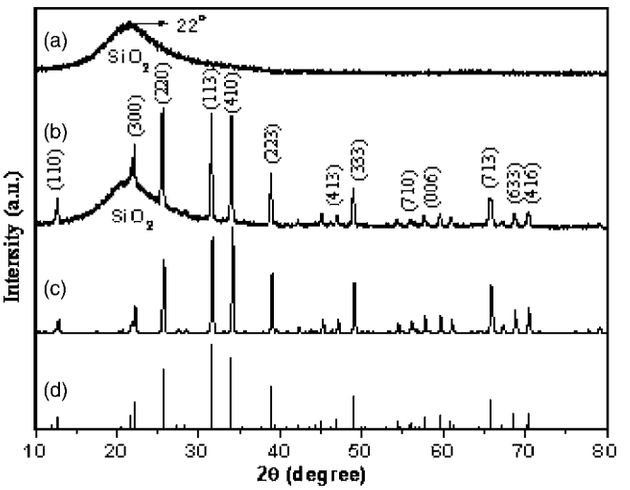

Figure 1. XRD patterns for (a) the 1000°C-annealed SiO_2, (b) Zn_2SiO_4:Mn@SiO_2 core-shell particles, (c) pure Zn_2SiO_4:Mn powder sample, and (d) the JCPDS card (no. 37-1485) for Zn_2SiO_4. Miller indices of diffracting lattice planes are also shown.

before the silica spheres were added. The other processes were the same. The above process was repeated several times to increase the thickness of Zn_2SiO_4:Mn shells.

Characterizations.— The X-ray diffraction (XRD) of the powder samples was examined on a Rigaku-Dmax-IIB using Cu Kα radiation (λ = 0.15405 nm). Fourier transform infrared (FTIR) spectra were measured with Perkin-Elmer 580B infrared spectrophotometer with the KBr pellet technique. The morphology and composition of the samples were inspected using field emission scanning electron microscope (FE-SEM, XL30, Philips), transmission electron microscope (TEM, JEOL-2010, 200 kV), and energy-dispersive X-ray spectroscopy (EDS, JEOL JXA-840). The photoluminescence (PL) and the cathodoluminescence (CL) spectra were taken on a Hitachi F-4500 spectrofluorimeter equipped with a 150 W xenon lamp, 172 nm vacuum-uv (VUV) lamp (self-made) and 1–6 kV electron gun (self-made) as the excitation sources, respectively. The luminescence decay curves were obtained from a Lecroy Wave Runner 6100 digital oscilloscope (1 GHz) using 250 nm laser (pulse width = 4 ns, gate = 50 ns) as the excitation source (Continuum Sunlite OPO). All the measurements were performed at room temperature.

Results and Discussion

Formation and morphology of Zn_2SiO_4:Mn@SiO_2 core-shell particles.—*XRD*.—Figure 1 shows the XRD patterns for (a) the annealed SiO_2, (b) Zn_2SiO_4:Mn@SiO_2, and (c) pure Zn_2SiO_4:Mn powder samples, as well as (d) the JCPDS card (no. 37-1485) for Zn_2SiO_4 as a reference. For SiO_2 particles annealed at 1000°C (Fig. 1a), no diffraction peak is observed except for a broad band centered at 2θ = 22°, which is the characteristic peak for amorphous SiO_2 (JCPDS 29-0085). For the Zn_2SiO_4:Mn@SiO_2 composite phosphors fired at 1000°C (Fig. 1b), besides the broad band at 2θ = 22° from the amorphous SiO_2, all the diffraction peaks belonging to crystalline willemite (α-Zn_2SiO_4, JCPDS card 37-1485) (Fig. 1d) are present, indicating that the coating layer of Zn_2SiO_4:Mn has crystallized well on the surface of silica spheres. This agrees well with the situation for the pure Zn_2SiO_4:Mn powder annealed at 1000°C (Fig. 1c, in which well-crystalline Zn_2SiO_4 is observed). No other phase can be detected. Formation of the Zn_2SiO_4:Mn layer is due to the reaction of Zn^{2+}, Mn^{2+} ions (on silica surfaces) with SiO_2 cores at high temperature (1000°C), as shown in Scheme 1. In the Pechini process, the citric acid first formed chelate complexes with Zn^{2+} and Mn^{2+}, then the left carboxylic acid groups in the citric acid reacted

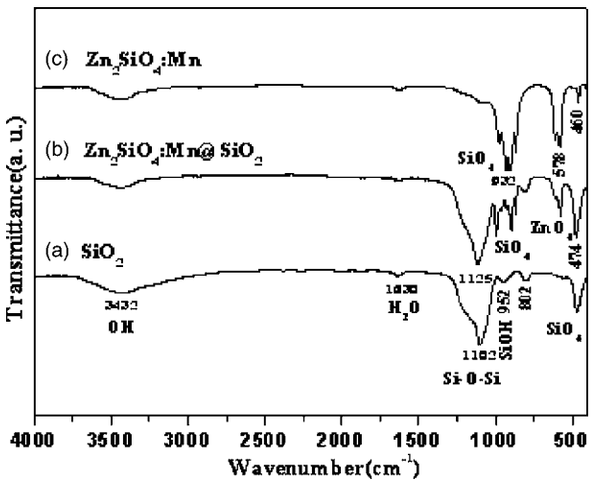

Figure 2. FTIR spectra of (a) the as-formed SiO_2, (b) 1000°C-annealed Zn_2SiO_4:Mn@SiO_2 core-shell sample, and (c) pure Zn_2SiO_4:Mn powder.

with PEG to form polyester with a suitable viscosity. The Zn^{2+} and Mn^{2+}, stabilized by the chelating and polymerizing process, were homogeneously distributed in the solution.[28] The Stöber process-derived silica particles contained a large amount of free hydroxyl groups (-OH) and silanol groups (Si–OH) on their surface (evidenced by FTIR spectra, see next section). By stirring silica particles in the solution, a lot of Zn^{2+} and Mn^{2+} were absorbed onto the silica particles by physical and chemical interactions. After the drying and annealing process, the Zn^{2+} and Mn^{2+} reacted with surface SiO_2 to form a Zn_2SiO_4:Mn layer on the silica cores.

FTIR.—The FTIR spectra of the as-formed SiO_2, 1000°C fired Zn_2SiO_4:Mn@SiO_2 core-shell sample, and pure Zn_2SiO_4:Mn powder are shown in Fig. 2a-c, respectively. In Fig. 2a for the as-formed SiO_2 particles, the absorption bands and their corresponding vibrational models are 3432 cm^{-1} (ν_1, O–H), 1630 cm^{-1} (O–H in H_2O), 1102 cm^{-1} (ν_3, Si–O–Si), 952 cm^{-1} (ν_1, Si–OH), 802 cm^{-1} (ν_1, Si–O–Si), 474 cm^{-1} (ν_4, Si–O), where ν_1 is symmetric stretching, ν_3 is asymmetric stretching, and ν_4 is asymmetric deformation vibrations, respectively.[29-32] This indicates that the as-formed SiO_2 particles contain a large amount of OH groups and H_2O on their surfaces. The surface Si–OH groups play an important role for bonding the metal ions from the coating sol and forming the Zn_2SiO_4:Mn layer on the SiO_2 surfaces in the following annealing process, as shown in Scheme 1. In Fig. 2b for the Zn_2SiO_4:Mn@SiO_2 core-shell sample, apart from the absorption peaks from silica cores (1125, 474 cm^{-1}), the characteristic absorption peaks due to SiO_4 (ν_1, 995, 894 cm^{-1}) and ZnO_4 (ν_3, 577 cm^{-1} from crystallized Zn_2SiO_4 are present.[33,34] These absorption peaks are basically similar to those for the pure Zn_2SiO_4:Mn sample, as shown in Fig. 2c. This suggests that crystalline phase (Zn_2SiO_4) has formed after annealing at 1000°C, agreeing well with the results of XRD and further demonstrating the formation of crystalline Zn_2SiO_4:Mn coating layers on the silica surfaces via the sol-gel process and annealing treatment. Note that weak OH vibration can be found in Zn_2SiO_4:Mn@SiO_2 and Zn_2SiO_4:Mn samples due to the absorption of traces of water in the course of measurement.

FESEM, EDS, TEM.—Figure 3 shows the FE-SEM micrographs of (a) the as-formed SiO_2 particles, (b) the single Zn_2SiO_4:Mn layer coated SiO_2 core-shell (Zn_2SiO_4:Mn@SiO_2) particles annealed at 1000°C, and (c) the EDS of Zn_2SiO_4:Mn@SiO_2 sample. From the FESEM micrograph of Fig. 3a we can observe that the as-formed SiO_2 particles are monodisperse spheres with smooth surfaces and nonaggregation, whose average size (in diameter) is about 750 nm.

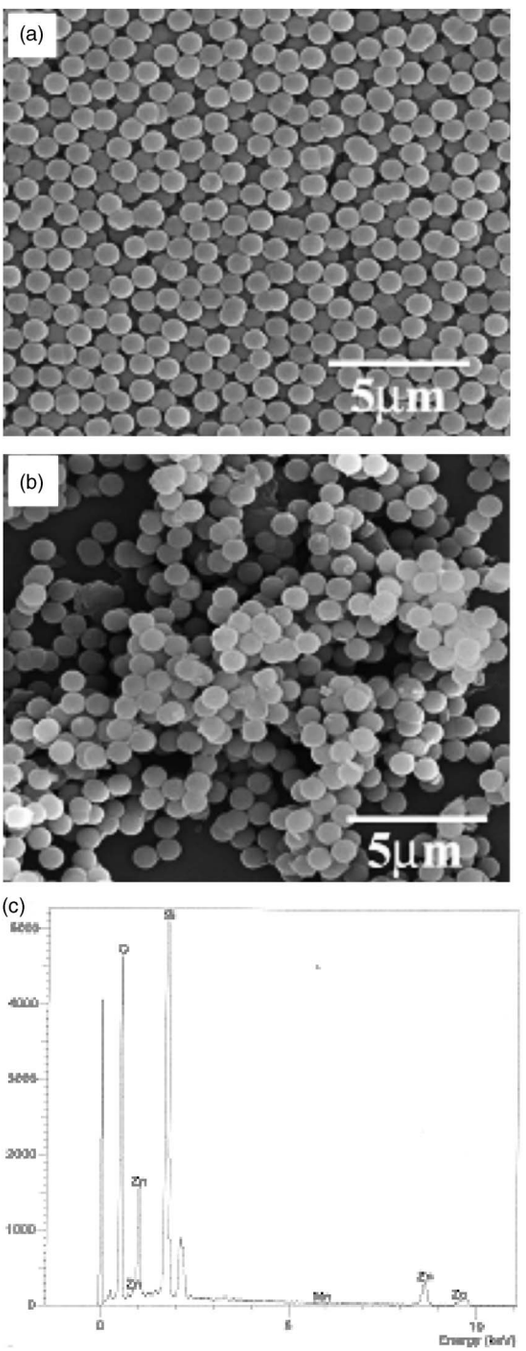

Figure 3. FE-SEM micrographs of (a) the as-formed SiO_2 particles, (b) the 1000°C-annealed core-shell Zn_2SiO_4:Mn@SiO_2 particles, and (c) EDS of Zn_2SiO_4:Mn@SiO_2 sample.

The core-shell Zn_2SiO_4:Mn@SiO_2 particles (Fig. 3b) are also uniform spheres with a little aggregation, whose average size (diameter) seems larger than the pure SiO_2 particles due to the extra layers of Zn_2SiO_4:Mn on the SiO_2 spheres. However, it should be mentioned that the FE-SEM micrographs can only provide the basic information on the morphology of Zn_2SiO_4:Mn@SiO_2 particles in large scale, and the core-shell structure of Zn_2SiO_4:Mn@SiO_2 particles cannot be resolved from the FE-SEM micrographs. To further confirm the existence of Zn_2SiO_4:Mn layers on the surfaces of silica particles, EDS was performed on the sample in Fig. 3b, as shown in

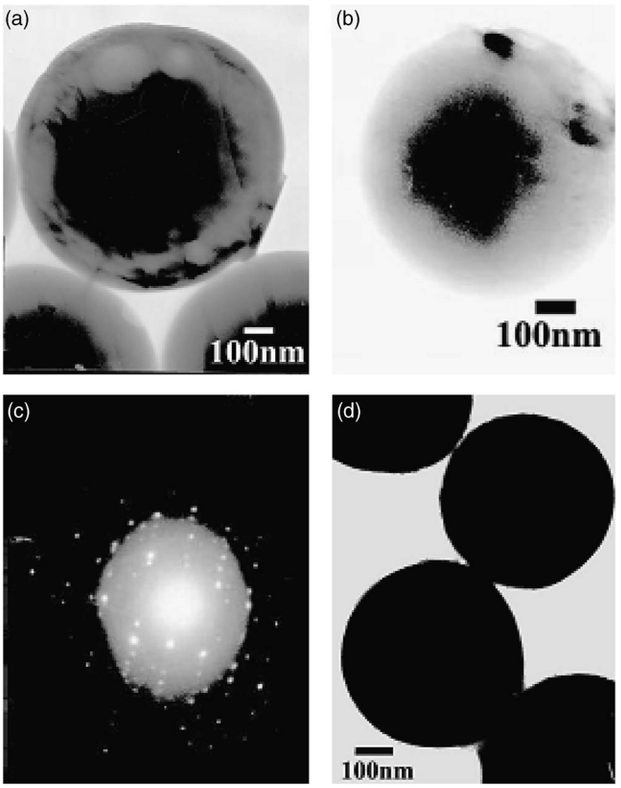

Figure 4. TEM micrographs for 1000°C-annealed (a) single and (b) double layer of Zn_2SiO_4:Mn-coated SiO_2 particles and (d) the bare SiO_2 particles as well as (c) the electron-diffraction pattern for (a).

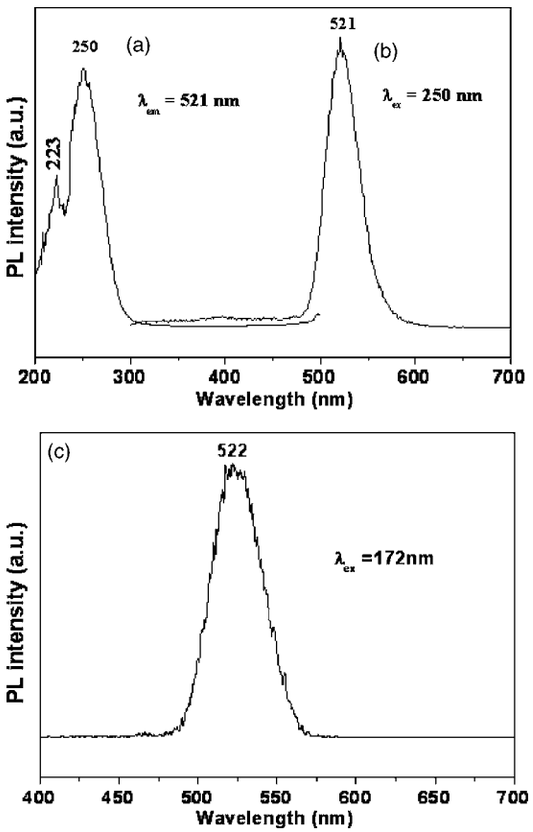

Figure 5. (a) Excitation and (b, c) emission spectra of (single-layer) Zn_2SiO_4:Mn@SiO_2 core-shell particles.

Fig. 3c. Si, Zn, and O elements were detected on the surface of the complex particles. The Mn element was not detected clearly due to its low concentration (but it can be detected by the emission spectra, see next part). This provides additional evidence for the formation of coatings of crystalline Zn_2SiO_4:Mn on the SiO_2 particles.

In order to see the core-shell structure of Zn_2SiO_4:Mn@SiO_2 particles, TEM was performed. Representative TEM micrographs are shown for the SiO_2 particles coated by one and two layers of Zn_2SiO_4:Mn shell in Fig. 4a and b, respectively. In both cases, the core-shell structure for the Zn_2SiO_4:Mn@SiO_2 particles can be seen clearly due to the different electron penetrability for the cores and shells. The cores are black and the shells have gray color. The core-shell Zn_2SiO_4:Mn@SiO_2 particles remain spherical. The average thickness for a single-layer shell is about 150 nm (Fig. 4a), and that for a double-layer shell is about 220 nm (Fig. 4b). Obviously, the shell thickness increases with the increase of the number of coating times. As a comparison, no such kind of core-shell structure can be observed in bare SiO_2 particles, as shown in Fig. 4d. Fig. 4c shows the electron-diffraction pattern performed on the surface of the particles in Fig. 4a, which clearly demonstrates the formation of crystalline phase. Combined with the results of XRD in Fig. 1a, we can know that this crystalline phase must be Zn_2SiO_4:Mn. In summary, from the results of FE-SEM, EDS, and TEM, it can be concluded that Zn_2SiO_4:Mn layers have crystallized on the surface of SiO_2 spheres to form Zn_2SiO_4:Mn@SiO_2 core-shell particles, which mainly keep the original spherical morphology of the SiO_2 particles.

Luminescent and kinetic properties of Zn_2SiO_4:Mn@SiO_2 core-shell particles.—Upon UV and VUV light excitation, the Zn_2SiO_4:Mn@SiO_2 core-shell particles exhibit strong green luminescence. Figure 5 shows the (a) excitation and (b, c) emission spectra of the core-shell particles annealed at 1000°C, respectively. The excitation spectrum (Fig. 5a) contains an intense broad band with a maximum at 250 nm (5.0 eV) and a narrow shoulder at 223 nm (5.6 eV) extended to the VUV region (below 200 nm, not shown). The former corresponds to the charge-transfer band (CTB) of Mn^{2+} ion, and the latter originates from the absorption of the host lattice of Zn_2SiO_4. This indicates that an energy transfer occurs from the Zn_2SiO_4 host lattice to Mn^{2+}.[20-26] Excitation into the CTB of Mn^{2+} at 250 nm or host band at 172 nm yields the emission spectrum with a maximum at 521–522 nm (Fig. 5b and c), which corresponds to the typical $^4T_1(^4G)$-$^6A_1(^6S)$ transition of Mn^{2+}. The green emitting can be explained when it is assumed that Mn^{2+} ions occupy a part of Zn^{2+} sites with four oxygen coordinated. The weak crystal field around Mn^{2+} results in the low splitting width of its 3d energy levels, and an emission at high energy (green) is observed. The mechanism involved in the green emission of Mn^{2+} in Zn_2SiO_4 is shown in Fig. 6. Under excitation of 250 nm UV, an electron from

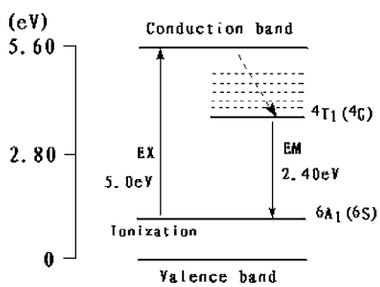

Figure 6. The PL mechanism for Mn^{2+} in Zn_2SiO_4.

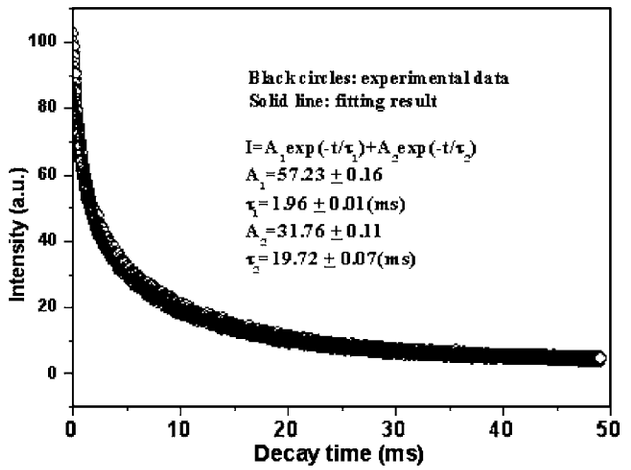

Figure 7. The decay curve for the $^4T_1(^4G)$–$^6A_1(^6S)$ (521 nm) emission of Mn^{2+} in (single layer) Zn_2SiO_4:Mn@SiO_2 sample annealed at 1000°C.

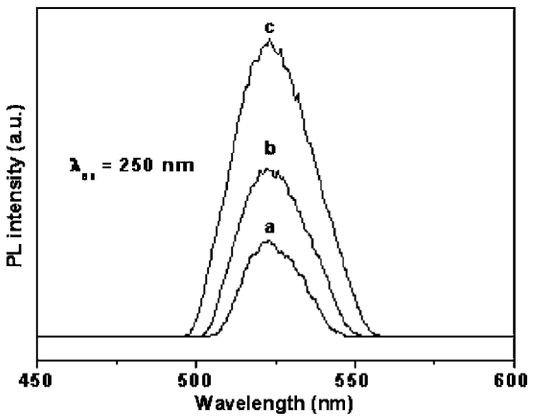

Figure 8. The PL emission intensity of Mn^{2+} in Zn_2SiO_4:Mn@SiO_2 sample as a function of the coating number (N): (a) $N = 1$, (b) $N = 2$, and (c) $N = 3$.

the Mn^{2+} ground state $^6A_1(^6S)$ is excited to the conduction band (CB) of Zn_2SiO_4. The process can be expressed as $Mn^{2+} + h\nu \rightarrow Mn^{3+} + e$, where $h\nu$ is the energy required in the photoexcitation of Mn^{2+}. The free electrons in the CB can relax to the $^4T_1(^4G)$ excited states of Mn^{2+} through a nonradiative process, then radiative transition from $^4T_1(^4G)$ excited state to the ground state $^6A_1(^6S)$ occurs, resulting in the green emission of Mn^{2+} at 521 nm.[35]

In order to study the decay behavior of Mn^{2+} luminescence in more detail in the Zn_2SiO_4:Mn@SiO_2 core-shell particles, the kinetic curve for the representative emission of Mn^{2+} $^4T_1(^4G)$-$^6A_1(^6S)$ (521 nm) was measured, as shown in Fig. 7. The decay curve can be well fitted into a double exponential function as $I = A_1 \exp(-t/\tau_1) + A_2 \exp(-t/\tau_2)$, and the fitting results are shown inside Fig. 7. Two lifetimes, a fast one $\tau_1 = 1.96$ ms and a slow one $\tau_2 = 19.7$ ms have been obtained for the emission of Mn^{2+}. The lattice of zinc silicate (Zn_2SiO_4) with willemite structure consists of corner-joined tetrahedral groups of [SiO_4] and [ZnO_4]. This structure contains two kinds of Zn^{2+} sites, both having four nearest-neighbor oxygens in a slightly distorted tetrahedral configuration. Accordingly, it can be assumed that the Mn^{2+} ions occupy the two different Zn^{2+} sites in the crystalline layer of Zn_2SiO_4 in the Zn_2SiO_4@SiO_2 core-shell particles, and the two different lifetimes arise from the Mn^{2+} ions occupied in the two different sites.[36] The average lifetime of Mn^{2+} $^4T_1(^4G)$-$^6A_1(^6S)$ emission, defined as $\langle\tau\rangle = (A_1\tau_1^2 + A_2\tau_2^2)/(A_1\tau_1 + A_2\tau_2)$, can be determined to be 17 ms.[37] The long lifetime of Mn^{2+} is due to the forbidden properties of the electronic transitions within $3d^5$ configuration of Mn^{2+}.[20]

The PL intensity of Zn_2SiO_4:Mn@SiO_2 core-shell particles can be tuned by the number of coatings. Figure 8 shows PL intensity as a function of the number of coatings. Clearly the PL intensity of Zn_2SiO_4:Mn@SiO_2 core-shell particles increases with raising the coating number. Obviously this can be attributed to the increase of the thickness of Zn_2SiO_4:Mn shells on the SiO_2 spheres. At present the PL intensity of three-layer Zn_2SiO_4:Mn@SiO_2 particles is still not as strong as that of the pure Zn_2SiO_4:Mn sample, but this might be overcome by further coating and optimizing other experimental conditions such as annealing temperature and time as well as the doping concentration of Mn^{2+}, which are underway.

The Zn_2SiO_4:Mn@SiO_2 core-shell particles also show a strong green emission under low-voltage cathode ray excitation, and the resulted CL spectra are identical with those of the PL emission spectra shown in Fig. 5b and c due to the $^4T_1(^4G)$-$^6A_1(^6S)$ transition of Mn^{2+}. The CL emission intensity for one-layer Zn_2SiO_4:Mn-coated SiO_2 particles has been investigated as a function of filament current and accelerating voltage, as shown in Fig. 9a and b, respectively. Under 4 kV electron-beam excitation, the CL intensity increases with increasing the filament current from 14 to 18 mA (Fig. 9a). Similarly, when the filament current is fixed at 14 mA, the CL intensity also increases with raising the accelerating voltage from 1 to 6 kV (Fig. 9b).

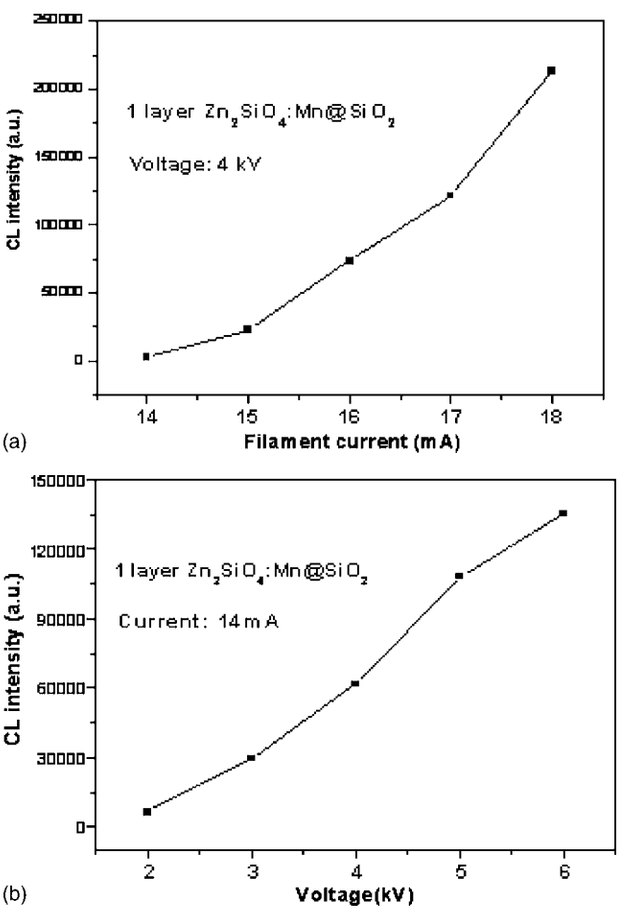

Figure 9. The CL emission intensity of Mn^{2+} as a function of (a) filament current and (b) accelerating voltage.

Conclusions

Spherical core-shell structured Zn_2SiO_4:Mn@SiO_2 particles with uniform size distribution have been successfully prepared by the sol-gel method followed by annealing at high temperature. Upon UV, VUV, and cathode ray excitation, the luminescence properties of the Zn_2SiO_4:Mn@SiO_2 core-shell particles are typical of those of Zn_2SiO_4:Mn, i.e., green band emission at 521 nm due to $^4T_1(^4G)$-$^6A_1(^6S)$ transition of Mn^{2+}. The PL intensity of the core-shell particles can be tuned by the number of coatings. With the increase of the number of coatings, the PL intensity increases. The CL intensity of the Zn_2SiO_4:Mn@SiO_2 particles increases with raising the filament current and cathode voltage. The advantages of the phosphors prepared by this process are the easy availability of homogeneous spherical morphology in different size, and its wide practicality for other phosphor materials.

Acknowledgments

This project is financially supported by the foundation of "Bairen Jihua" of the Chinese Academy of Sciences, the MOST of China (no. 2003CB314707), and the National Natural Science Foundation of China (NSFC; 50225205, 20271048, 20431030). Professor J. Fang is grateful for the financial support by the foundation of a two-base program for international cooperation of NSFC (00310530) related to project 50225205, and NSF DMR-0449580. We are grateful for Professor Yingnimg Yu and Liaohai Ge for measuring the decay curve and TEM, respectively.

References

1. R. A. Caruso and M. Antonietti, *Chem. Mater.*, **13**, 3272 (2001).
2. F. Caruso, M. Spasova, and V. Salgueirno-Maceria, *Adv. Mater. (Weinheim, Ger.)*, **13**, 1090 (2001).
3. H. Giesche and E. Matijevic, *J. Mater. Res.*, **9**, 436 (1994).
4. H. Sertchook and D. Avnir, *Chem. Mater.*, **15**, 1690 (2003).
5. M. Giersig, T. Ung, L. M. Liz-Marzan, and P. Mulvaney, *Adv. Mater. (Weinheim, Ger.)*, **9**, 570 (1997).
6. M. Ocana, W. P. Hsu, and E. Matijevic, *Langmuir*, **7**, 2911 (1991).
7. W. P. Hsu, R. C. Yu, and E. Matijevic, *J. Colloid Interface Sci.*, **156**, 56 (1993).
8. M. S. Fleming, T. K. Mandal, and D. R. Walt, *Chem. Mater.*, **13**, 2210 (2001).
9. P. Schuetzand and F. Caruso, *Chem. Mater.*, **14**, 4509 (2002).
10. S. R. Hall, S. A. Davis, and S. Mann, *Langmuir*, **16**, 1454 (2000).
11. I. Sondi, T. H. Fedynyshyn, R. Sinta, and E. Matijevic, *Langmuir*, **16**, 9031 (2000).
12. M. I. Martinez-Rubio, T. G. Ireland, G. R. Fern, J. Silver, and M. J. Snowden, *Langmuir*, **17**, 7145 (2001).
13. A. Vecht, C. Gibbons, D. Davies, X. Jing, P. Marsh, T. G. Ireland, J. Silver, and A. Newport, *J. Vac. Sci. Technol. B*, **17**, 750 (1999).
14. K. Y. Jung, D. Y. Lee, Y. C. Kang, and H. D. Park, *J. Lumin.*, **105**, 127 (2003).
15. Y. C. Kang, I. W. Lenggoro, S. B. Park, and K. Okuyama, *Mater. Res. Bull.*, **35**, 789 (2000).
16. A. Celikkaya and M. Akinc, *J. Am. Ceram. Soc.*, **73**, 2360 (1990).
17. W. Stöber, A. Fink, and E. Bohn, *J. Colloid Interface Sci.*, **26**, 62 (1968).
18. M. Yu, J. Lin, J. Fu, H. J. Zhang, and Y. C. Han, *J. Mater. Sci.*, **13**, 1413 (2003).
19. M. Yu, J. Lin, Z. Wang, J. Fu, S. Wang, H. J. Zhang, and Y. C. Han, *Chem. Mater.*, **14**, 2224 (2002).
20. G. Blasse, and B. C. Grabmaier, *Luminescent Materials*, Springer-Verlag, Berlin, Heidelberg (1994).
21. X. Ouyang, A. H. Kitai, and T. Xiao, *J. Appl. Phys.*, **79**, 3229 (1996).
22. T. S. Copeland, B. I. Lee, J. Qi, and A. K. Elrod, *J. Lumin.*, **97**, 168 (2002).
23. T. S. Ahmadi, M. Haase and H. Weller, *Mater. Res. Bull.*, **35**, 1869 (2000).
24. Y. C. Kang and S. B. Park, *Mater. Res. Bull.*, **35**, 1143 (2000).
25. A. Roy, S. Polarz, S. Rabe, B. Rellinghaus, H. Zähres, F. E. Kruis, and M. Driess, *Chem.-Eur. J.*, **10**, 1565 (2004).
26. R. P. Sreekanth Chakradhar, B. M. Nagabhushana, G. T. Chandrappa, K. P. Ramesh, and J. L. Rao, *J. Chem. Phys.*, **121**, 10250 (2004).
27. X. Wang, C. J. Summers, and Z. L. Wang, *Adv. Mater. (Weinheim, Ger.)*, **16**, 1215 (2004).
28. M. Kakihana and K. Domen, *MRS Bull.*, **25**(9), 27 (2000).
29. A. Kioul and L. Mascia, *J. Non-Cryst. Solids*, **175**, 169 (1994).
30. S. Kook Mah and I. J. Chung, *J. Non-Cryst. Solids*, **183**, 252 (1995).
31. Y. Chen and J. O. Iroh, *Chem. Mater.*, **11**, 1218 (1999).
32. J. Méndez-Vivar and A. Mendoza-Bandala, *J. Non-Cryst. Solids*, **261**, 127 (2000).
33. C. C. Lin and P. Y. Shen, *J. Non-Cryst. Solids*, **171**, 281 (1994).
34. A. M. Pires and M. R. Davolos, *Chem. Mater.*, **13**, 21 (2001).
35. R. Selomulya, S. Ski, and K. Pita, *Mater. Sci. Eng., B*, **100**, 136 (2003).
36. A. Patra, G. A. Baker, and S. N. Baker, *J. Lumin.*, **111**, 105 (2005).
37. S. Murakami, M. Herren, D. Rau, and M. Morita, *Inorg. Chim. Acta*, **300–302**, 1014 (2000).